Progress In Electromagnetics Research Letters, Vol. 24, 177–185, 2011

MULTIPACTOR ON A DIELECTRIC SURFACE WITH LONGITUDINAL RF ELECTRIC FIELD ACTION

F. Zhu*, Z. Zhang, J. Luo, and S. Dai

Key Laboratory of High Power Microwave, Institute of Electronics, Chinese Academy of Sciences, Beijing 100190, China

Abstract—An improved multipactor dynamic model is proposed for studying the multipactor phenomenon on a dielectric surface existing longitudinal RF electric field using Monte Carlo method. The susceptibility curves of the electric field on the surface and the temporal evolution images of the multipactor discharge were obtained and discussed. The power deposited on the dielectric surface by the multipactor was also investigated in terms of an S-band RF dielectric window. The results show that, the longitudinal RF electric field may intensify the single-surface multipactor effect, which is likely detrimental to RF transmission and to result in the dielectric crack.

1. INTRODUCTION

The multipactor effect is a resonant vacuum electron discharge that can occur in high power microwave devices, such as dielectric windows. Studies on the multipactor discharges on a dielectric surface in recent years have mainly focused on both the multipactor breakdown voltage threshold, thus leading to the construction of generalized susceptibility curves, as well as the time evolution of the discharge and its saturation mechanism, in terms of the external transverse RF electric field and of the dc electric field [1, 2]. However, experiments and theoretical study show that high-order mode containing longitudinal RF electric field may be excited on the window surface because of the sharp change of the boundary conditions, and the magnitude of this field component may be much higher than that of the dc electric field at the initial stage of multipactor [3–5]. Therefore, it is very important to develop a particular model to better understand the single-surface multipactor process with the longitudinal RF electric field.

Received 23 April 2011, Accepted 13 June 2011, Scheduled 16 June 2011

* Corresponding author: Fang Zhu (zhufang06@mails.gucas.ac.cn).

In this article, we extend the analysis of the previous work by studying the susceptibility diagrams and the time evolution of the multipactor discharges on a dielectric surface on the base of the consideration of the transverse and longitudinal RF electric field as well as the dc electric field at the same time. The influence of longitudinal RF electric field on the multipactor effect is emphasized, and the temperature increase on an S-band alumina window disk caused by both multipactor and dielectric-losses is evaluated.

2. THE MODEL AND THEORY

The geometry of the single-surface multipactor under investigation is shown in Fig. 1. Electrons emitted with a random velocity, v_0, and a random angle, ϕ, with respect to the positive y-axis, are subjected to forces imposed by the transverse component $E_y = E_{\mathrm{y0}} \sin(\omega t + \theta)$, the longitudinal component $E_z = E_{\mathrm{Z0}} \cos(\omega t + \theta)$ of the RF electric field, and the initial dc electric field. The electron gains energy from the RF electric field in its transit process and strikes the surface with much larger energy at a later time. Upon impact, a number of secondary electrons are emitted. Thus, a time-varying positive static field normal to the dielectric surface, namely the dc electric field E_{dc}, is build up. Suppose that the positive charge left on the dielectric surface is uniformly distributed, $E_{dc} = E_{dc0} + eN_e/2A\varepsilon_0$ where E_{dc0} is the initial dc electric field, N_e is the total number of multipactor electrons in flight, A is the surface area of the dielectric, and ε_0 is the free space permittivity.

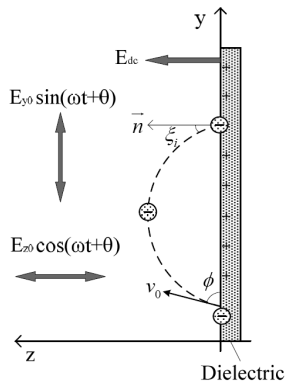

Figure 1. Schematic of single-surface multipactor in transverse/longitudinal RF and dc electric fields.

To investigate the influence of the longitudinal RF electric field on the multipactor process, two different scenarios shall be analyzed for the electron dynamics as follows:

(1) In the absence of the longitudinal RF component, only the transverse RF electric field, E_y, and the dc electric field, E_{dc1}, exist on the dielectric surface, which is identical to the condition in Refs. [1, 2].

$$\begin{aligned} v_{y1} &= v_0 \cos\phi + \frac{e}{m\omega} E_{y0}[\cos(\omega\tau_1 + \theta) - \cos\theta] \\ v_{\mathrm{Z}1} &= v_0 \sin\phi - \frac{e}{m} E_{\mathrm{dc}1}\tau_1 \\ \tau_1 &= \frac{2mv_0 \sin\phi}{eE_{\mathrm{dc}1}} \end{aligned} \tag{1a}$$

(2) Both the transverse and longitudinal RF electric field, E_y and E_z, as well as the dc electric field, E_{dc2}, are considered. The equations of the motion of secondary electrons based on the multipactor dynamic model shown in Fig. 1 can be given as below:

$$\begin{aligned} &v_{y2} = v_0 \cos\phi - \frac{e}{m}\int_0^{\tau_2} E_{y0}\sin(\omega t + \theta)dt \\ &v_{z2} = v_0 \sin\phi - \frac{e}{m}\int_0^{\tau_2} [E_{z0}\cos(\omega t + \theta) + E_{\mathrm{dc}2}]dt \\ &v_0 \sin\phi \cdot \tau_2 + \frac{eE_{\mathrm{Z}0}}{m\omega^2}[\cos(\omega\tau_2 + \theta) - \omega\tau_2 \sin(\omega\tau_2 + \theta) - \cos\theta] \\ &- \frac{eE_{\mathrm{dc}2}}{2m}\tau_2^2 = 0 \end{aligned} \tag{1b}$$

where v_y and v_z are the y and z component of the impact velocity, τ is the transit time, e/m is the ratio of the electron charge to its mass, $= 1.76 \times 10^{11}$. Solving Equation (1), the impact energy, W_i, and the impact angle, ξ_i, of the electron may easily be calculated from $W_i = \frac{1}{2}m(v_y^2 + v_z^2)$ and $\xi_i = \arctan(\sqrt{v_y/v_z})$.

Upon impact on the surface, a primary electron produces an average number of secondary electrons, called the secondary electron yield (SEY), δ. This yield depends on the material, and is a function of the impact energy of the primary electron, W_i, and the impact angle, ξ_i, at which it strikes the surface [6, 7]. The SEY prosperities for the material used in the simulation are defined by the following parameter: $\delta_{\max 0} = 3.0$ and $W_{\max 0} = 420\,\mathrm{eV}$, respectively, where $\delta_{\max 0}$ is the maximum value of the SEY function for normal incidence, and $W_{\max 0}$ is the corresponding impact energy of the electron.

In the specific cases studied in this paper, Monte Carlo method is employed to simulate the multiplication of the electrons on the dielectric surface. The secondary electron departure kinetic energy W_o ($= 1/2 mv_0^2$) and angle ϕ are assumed to follow the probability density functions as below: [1, 2]

$$f(W_o) = \frac{W_o}{W_{om}^2} \exp\left(\frac{-W_o}{W_{om}}\right)$$
$$g(\phi) = \frac{1}{2} \sin\phi \tag{2}$$

With $W_{om} = 2.1\,\text{eV}$ being the peak of the distribution of departure energies.

3. RESULTS AND DISCUSSION

The susceptibility diagrams identify the domain of the electric field amplitudes in which the multipactor would occur. Since the SEY is above unity only for the electron impact energies between the two crossover points, there are upper and lower boundaries where $\delta = 1$. Fig. 2 shows such boundary regions with $\delta_{\max 0} = 3.0$, $W_{\max 0} = 420\,\text{eV}$ under the two scenarios of Equation (1). The vertical axis denotes the normalized value of E_{y0}, and the horizontal axis denotes the normalized value of E_{dc1} when the longitudinal RF electric field is not considered, or that of the electric field superposition, $E_{z0} + E_{dc2}$, when the particular field E_z is included.

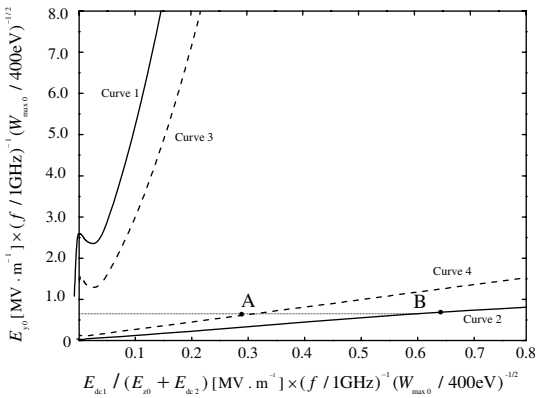

Figure 2. Multipactor region boundaries versus the electric field intensity for $\delta_{\max 0} = 3.0$ (dashed line) when the longitudinal RF field is not considered and (solid line) when it is included on a dielectric surface.

As shown in Fig. 2, either E_{dc1} or $(E_{z0} + E_{dc2})$ increases approximately linearly with the increase of E_{y0}. However, the susceptible domain of the multipactor discharge between Curve 1&2 is wider than that between Curve 3&4, i.e., the values of the field amplitudes falling outside Curve 3&4 may still lie within Curve 1&2. The extension of the multipactor region including the effects of the longitudinal RF electric field may be explained as follows: in the first scenario of Equation (1), the dc electric field E_{dc1} has an unchanged direction pointing to the outside surface. While in the other scenario, when the value of E_{z0} is larger than that of the E_{dc2}, the direction of the compositive field $(E_{z0} + E_{dc2})$ may be opposite to the dc field due to the RF swing. The dc electric field always attracts the secondary electrons back to the surface, while the total longitudinal field may repel the electrons flying away from the surface, thus increase the averaged transit time of the electrons. This repulsion action may greatly be intensified in the case of no dc electric field but just the longitudinal RF field existing on the surface. Now for a given value of the transverse RF electric field on the lower boundary, the impact energy of the secondary electrons will increase in the transit process because of the action of the longitudinal superposition field, which eventually leads to the extension of the susceptible regions.

For an S-band alumina window, we set the area A to be $12\,\mathrm{cm}^2$, and the longitudinal RF electric field to be a magnitude of about 40% of the transverse component [2, 5]. The time evolution images of multipactor discharge with/without the effects of the longitudinal RF electric field were given in Fig. 3 using following input parameters:

$$\begin{aligned} &\delta_{\max 0} = 3.0,\ W_{\max 0} = 420\,\mathrm{eV},\ W_{om} = 2.1\,\mathrm{eV},\ A = 12\mathrm{cm}^2 \\ &E_{y0} = 2.0\,\mathrm{MV/m},\ E_{z0} = 0.8\,\mathrm{MV/m},\ E_{dc0} = 10\,\mathrm{V/m}, \\ &f = \omega/2\pi = 3.0\,\mathrm{GHz} \end{aligned} \tag{3}$$

As Curve 1 shown in Fig. 3, when the longitudinal RF electric field effects are not considered, the simulation results are similar to those in Ref. [1, 2]. The number of multipactor electrons reaches a steady saturation value of $N_{e1} = 1.159 \times 10^{11}$ after about 40 collisions, at saturation, the secondary yield δ has a mean value of unity, the dc field building on the surface grows from the initial value of $E_{dc0} = 10\,\mathrm{V/m}$ to a large value of $E_{dc1} = 0.874\,\mathrm{MV/m}$, corresponding to point A on the susceptibility curve in Fig. 2, the impact energy of the electron, W_i, is near the first crossover energy of 28 eV in the SEY curve; the averaged impact angle, ξ_i, is about 75° and the averaged saturation transit time of electron is $\tau_1 = 1.17 \times 10^{-11}\,\mathrm{s}$.

When the longitudinal RF electric field effects are included, as Curve 2 shown in Fig. 3, the evolution of the multipactor discharge

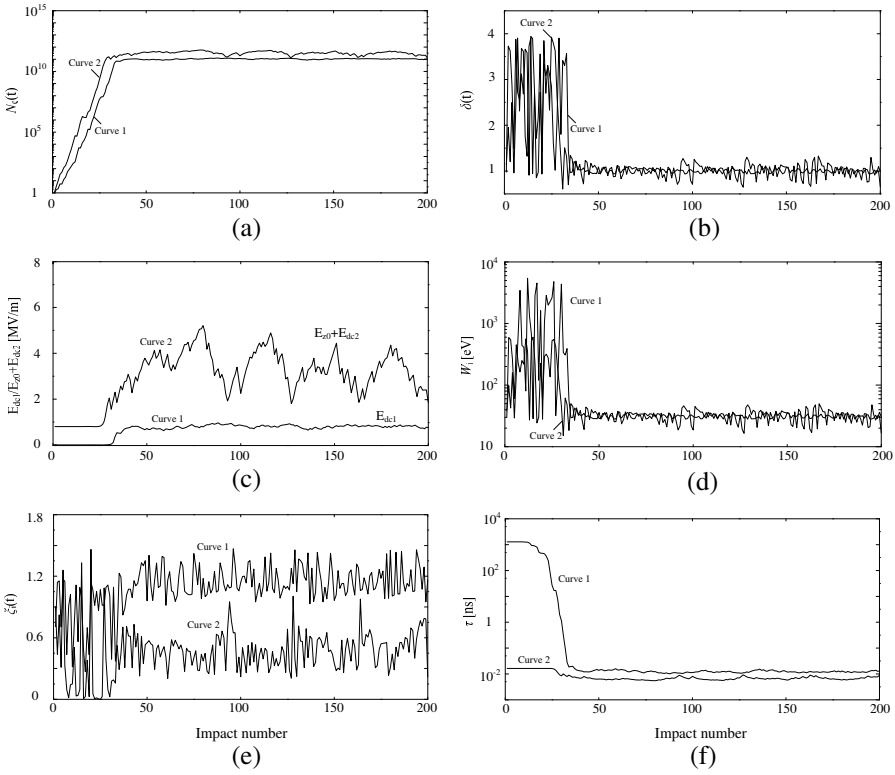

Figure 3. Evolution of multipactor discharge (Curve 1) when the longitudinal RF field is not considered and (Curve 2) when it is included on a dielectric surface.

generally showed some sort of periodicity at saturation, i.e., the values of the parameters shown in Figs. 3(a) $\sim$ 3(f) repeated almost regularly at about 40-collisions cycles. This periodicity exhibited more obviously in Figs. 3(a), (c), (e), (f), and not much clearly in Figs. 3(b), (d), while there were always peak values at certain intervals in Figs. 3(b) and (d) that also presented the same tendency. The reason leading to this phenomenon may be that, the presence of the longitudinal RF electric field makes the electron transit time, τ_2, have the periodicity at a certain extent, using Equation (1b), then the electron impact energy obtained in the transit process shall also be periodic, which consequently influenced the other parameters of the multipactor discharge.

As Curve 2 shown in Fig. 3, N_{e2} reaches a steady saturation level of 1.382×10^{11}, the amplitude of the compositive longitudinal electric field,

$E_{z0} + E_{dc2}$, increases to a larger value of 1.842 MV/m, superpositioned by $E_{z0} = 0.8$ MV/m and $E_{dc2} = 1.042$ MV/m, corresponding to point B on the susceptibility curve in Fig. 2, the impact angle of the secondary electron is decreased to 32° which shows an attracting action of the longitudinal fields on the multipactoring electron trajectories. The trends of the secondary yield [(Fig. 3(b)] and of the electron impact energy [(Fig. 3(d)] are almost as the same as those when just the dc electric field exists. The averaged saturation transit time of the electron is $\tau_2 = 0.856 \times 10^{-11}$ s. The averaged period of the evolution of the parameters in Fig. 3 then can be estimated as $T = 40 \times 0.856 \times 10^{-11}$ s $= 3.424 \times 10^{-10}$ s, which is corresponding to the RF cycle 1/3.0 GHz. As can be seen, with the influence of the longitudinal RF electric field, more secondary electrons are emitted, thus the amplitude of the dc electric field E_{dc2} is increased 19% than that of E_{dc1}, and the amplitude of the total longitudinal electric field is over 2 times than that of E_{dc1} in Fig. 3. When the amplitude of the longitudinal RF field, E_{z0}, is positive, the averaged transit time of the electron for the saturation status would be shortened over 50% due to the acceleration action. When E_{z0} is negative, which means the direction of the longitudinal RF field is opposite to that of the dc field ($E_{z0} > E_{dc2}$), it might make some secondary electrons flying away from the surface and prolong the transit time of the electrons. However, the averaged attracting action on electron of the longitudinal RF field is stronger than its repelling action due to the RF swing, therefore, the transit time of the electron in this scenario, $\tau_2 = 0.856 \times 10^{-11}$ s, is 27% decreased than $\tau_1 = 1.17 \times 10^{-11}$ s.

Using the simulated results given in Fig. 3, the amount of the power deposited on the dielectric surface by the multipactor could be estimated from $P_{m1} = N_{e1} \cdot W_{i1}/\tau_1 = 44.43$ kW, and $P_{m2} = N_{e2} \cdot W_{i2}/\tau_2 = 72.42$ kW. Usually, the heating of the dielectric mainly results from two aspects: one is the power deposited on the dielectric by the multipactor, and the other is the dielectric losses. In the steady state, the temperature increase, T, is governed by the time-independent diffusion equation in terms of the average power density of both the multipactor effect and the dielectric-losses: [4, 10]

$$-\lambda \cdot \nabla^2 T(z,r) = \frac{1}{2}\omega\varepsilon_0\varepsilon_r''\tau_f|E(z,r)|^2 + p_m \tag{4}$$

where λ is the thermal conductivity of 97% alumina, ε_0 is the free space permittivity, ε_r'' is the imaginary part of the relevant dielectric constant of the window disk, τ_f is the duty cycle, and p_m is the averaged power density by the multipactor discharge. By solving Equation (4) with the boundary conditions, we obtain the axial and radius temperature distribution with/without the effects of the longitudinal RF electric

field on the window disk (Fig. 4). The radius of the window disk cylinder is $R = 42\,\text{mm}$, and its thickness is $D = 3\,\text{mm}$. As shown in Fig. 4(a), when the longitudinal RF field is considered, the axial temperature distribution approximately increase an additional 35°C resulting from the excess electron-bombardment energy. While as observed in Fig. 4(b), the maximum-radial-temperature point moves 13.7 mm from the center to the edge of the ceramic. The radial temperature distributions generally vary more sharply than the axial temperature distributions. By such temperature gradients, a thermal stress will be produced inside the window disk and the magnitude of which is described by the following equation [8]:

$$\sigma_r = 1.4P\alpha\frac{(DR)^{1/2}}{l}(T_{\max} - T_{\min}) \tag{5}$$

where $P = 303\,\text{GPa}$ is the modulus of elasticity of the window disk, $\alpha = 8.2 \times 10^{-6}/°\text{C}$ is the coefficient of linear expansion ($10^{-6}/°\text{C}$), and l (mm) is the distance between the radial maximum and minimum temperature points on the dielectric. The thermal stresses including the longitudinal RF electric field effect or not, based on (5), are approximately 214.05 MPa and 97.44 MPa, respectively. The maximum tensile strength of the 97% alumina, however, is 179 MPa (strain rate of 10^{-6}m/s) [9]. Therefore, with the appearance of the longitudinal RF electric field, the thermal stress caused by radial temperature gradients produced by electron-bombardment and dielectric losses may exceed the maximum tensile strength of the ceramic, and lead to window failure.

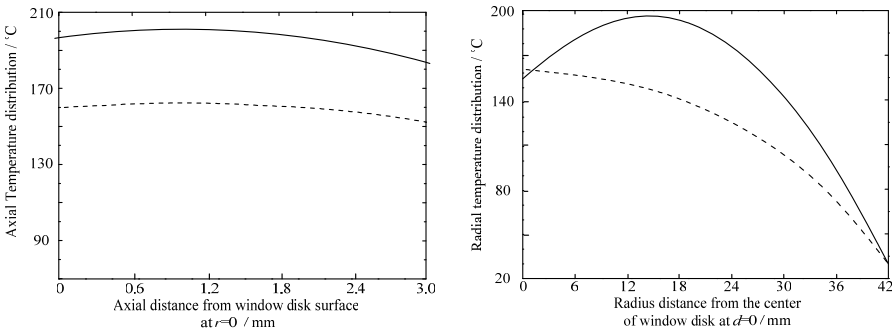

Figure 4. Temperature distribution (dashed line) when the longitudinal RF field is not considered and (solid line) when it is included.

4. CONCLUSION

In this paper, the susceptibility curves of multipactor over a range of operating conditions and the time evolution images have been calculated in order to study the influence of the longitudinal RF electric field on the single-surface multipactor discharge. The performed simulations suggest that, the main effects of the longitudinal RF electric field are to noticeably enlarge the susceptible domain of the multipactor discharge, to increase the number of the secondary electrons emitted from the dielectric surface to a much larger value, to accelerate the transit process of the electron, and to decrease the angles of the electron colliding the surface. The longitudinal RF electric field intensifies the electron bombardment and the power deposition on the dielectric surface, and is detrimental to thermal conduction and RF transmission for the dielectric windows.

REFERENCES

1. Kishek, R. A. and Y. Y. Lau, "Multipactor discharge on a dielectric," *Phys. Rev. Lett.*, Vol. 80, 193, 1998.
2. Ang, L.-K., Y. Y. Lau, R. A. Kishek, and R. M. Gilgenbach, "Power deposited on a dielectric by multipactor," *IEEE Trans. Plasma Sci.*, Vol. 26, 290, 2001.
3. Michizono, S., "Secondary electron emission from alumina RF windows," *IEEE Trans. Dielectr. Electr. Insul.*, Vol. 14, 583, 2007.
4. Bosman, H., Y. Y. Lau, and R. M. Gilgenbach, "Power absorption by thin films on microwave windows," *Appl. Phys. Lett.*, Vol. 82, 1353, 2003.
5. Zhu, F., Z. C. Zhang, J. R. Luo, and Y. W. Zhang, "Investigation of the failure mechanism for an S-band pillbox output window applied in high average power klystrons," *IEEE Trans. Electron Devices*, Vol. 57, 946, 2010.
6. Vaughan, J. R. M., "A new formula for secondary emission yield," *IEEE Trans. Electron Devices*, Vol. 36, 1963, 1989.
7. Vaughan, J. R. M., "Multipactor," *IEEE Trans. Electron Devices*, Vol. 35, 1172, 1988.
8. Preist, D. H. and R. C. Talcott, "On the heating of output windows of microwave tubes by electron bombardment," *IRE Trans. Electron Devices*, Vol. 8, 243, 1961.
9. Nemat-Nasser, S. and H. Deng, "Strain rate effect on brittle failure in compression," *Acta Metall. Mater.*, Vol. 42, 1013, 1994.
10. Ramo, S., J. R. Whinnery, and T. Van Duzer, *Fields and Waves in Communication Electronics*, 3rd edition, Wiley, New York, 1994.